JOURNAL OF THERMOPHYSICS AND HEAT TRANSFER
Vol. 21, No. 2, April–June 2007

Applicability of Phase Ray-Tracing Method for Light Scattering from Rough Surfaces

H. J. Lee* and Z. M. Zhang†
Georgia Institute of Technology, Atlanta, Georgia 30332-0405

DOI: 10.2514/1.26191

The ray-tracing method based on geometric optics, in which the intensity of light is traced during scattering, absorption, and multiple reflections, is a convenient tool in radiative heat transfer. Recent studies employed a modified ray-tracing method to trace the field amplitude and phase for light scattering from rough surfaces. Because phase is included, this method will be called the phase ray-tracing method hereafter. Phase ray-tracing method works well for multiple reflections inside smooth thin films, but its applicability for the prediction of the radiative properties of rough surfaces has not been established. The present study compares both the phase ray-tracing method and ray-tracing method with the Kirchhoff approximation for one-dimensional rough surfaces. Mueller matrix calculations are compared for both dielectric and highly reflecting surfaces. When characteristic lengths of roughness are much greater than the incident wavelength, the three methods yield essentially the same results. At small characteristic lengths, the phase ray-tracing method predicts coherent peaks resulting from wave interferences. However, the phase ray-tracing method always underpredicts the coherent peaks compared with the Kirchhoff approximation and, furthermore, fails to predict peaks for some elements. Therefore, the phase ray-tracing method cannot accurately model wave features of the light scattered from rough surfaces with small characteristic lengths due to its inherent assumption from geometric optics, that is, specular reflection at surface microfacets.

Nomenclature

c	=	scattering coefficient
E	=	electric field
f_r	=	bidirectional reflectance distribution function
I	=	intensity
$\boldsymbol{k}$	=	wave vector
m	=	Mueller matrix element
R	=	Fresnel reflection coefficient
$\boldsymbol{r}$	=	position vector
$\boldsymbol{S}$	=	Stokes vector
δ	=	phase difference
λ	=	wavelength in vacuum
ξ	=	interface profile or roughness height
σ	=	root-mean-square roughness
τ	=	autocorrelation length

Subscripts

coh	=	coherent
i	=	incidence
inc	=	incoherent
p or s	=	p or s polarization
r	=	reflection
t	=	tangent plane

Introduction

GEOMETRIC optics has been widely applied for many radiative and optical problems in which characteristic lengths are much larger than the wavelength of interest such that wave effects are negligible [1–4]. One application of geometric optics is to model radiative properties of a rough surface by tracing rays between irregularities or asperities on the surface [3–9]. Recent studies demonstrated that geometric optics is valid even when characteristic lengths of roughness are comparable to or less than the wavelength [10–13]. Although the applicability of geometric optics is larger than expected, characteristic lengths are often in microscale and can be much smaller than wavelengths, particularly for thermal radiation. Consequently, wave features such as diffraction or interference prevail, and geometric optics becomes invalid for small length scales.

Based on geometric optics, many researchers have developed methods to trace ray intensity using specular reflection at the interface, while focusing on the scattered energy distribution. Because the ray-tracing method (RTM) that deals with intensity cannot model wave features, it is valid for large characteristic lengths in an incoherent limit. However, a method that traces field amplitude with phase difference can account for wave features beyond the validity domain of geometric optics. For example, the reflectivity of a smooth surface coated with a thin film can be calculated when field amplitudes and phase differences between rays undergoing multiple reflections within the film are considered [3]. This ray-tracing method incorporates wave interferences and covers the thin-film optics regime and will be referred to as the phase ray-tracing method (PRTM) hereafter. It is necessary to distinguish PRTM from RTM because of their different applicable regimes, although both methods are based on the light ray concept within geometric optics. Most studies relevant to light scattering, especially in the area of heat transfer, treat geometric optics and RTM as synonymous [2–11].

Bruce [14,15] introduced the concept of PRTM as an extension of RTM to calculate the Mueller matrix elements for rough surfaces with large characteristic lengths. However, no comparison and clear distinction were made in these studies between RTM and PRTM. Although PRTM can address wave features for smooth surfaces with small characteristic lengths, its application for rough surfaces is still questionable. Therefore, the present study investigates the applicability of PRTM for both small and large characteristic lengths of rough surfaces. The Mueller matrix elements obtained from PRTM are compared with those from the Kirchhoff approximation (KA) and RTM, for one-dimensional (1-D) dielectric and highly reflecting surfaces with Gaussian roughness statistics.

Presented as Paper 3432 at the 9th AIAA/ASME Joint Thermophysics and Heat Transfer Conference, San Francisco, CA, 5–8 June 2006; received 26 June 2006; revision received 30 August 2006; accepted for publication 30 August 2006.

*Graduate Research Assistant, George W. Woodruff School of Mechanical Engineering.

†Associate Professor, George W. Woodruff School of Mechanical Engineering; zhuomin.zhang@me.gatech.edu. Associate Fellow AIAA.

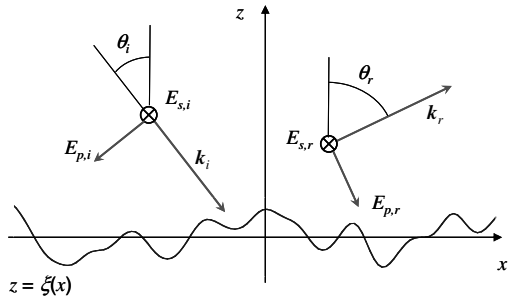

Fig. 1 Scattering geometry of a 1-D rough surface. The surface profile $\xi(x)$ separates an isotropic and homogeneous medium from a vacuum. The vacuum and the dielectric medium are surrounded by semi-infinite surfaces. Incident and scattered wave vectors are denoted by $k_i = k(\sin\theta_i, 0, -\cos\theta_i)$ and $k_r = k(\sin\theta_r, 0, \cos\theta_r)$, respectively.

Because KA in physical optics addresses wave features related to scattering and KA reduces to geometric optics in the short wavelength limit, the applicability of PRTM for small length scales can be evaluated by comparison with KA.

Fundamentals of Light Scattering

The reflection of a monochromatic plane wave $\boldsymbol{E}_i(\boldsymbol{r}) = \hat{\boldsymbol{y}} E_i e^{i\mathbf{k}_i\cdot\mathbf{r}}$ from a 1-D randomly rough surface is depicted in Fig. 1. The surface profile $\xi(x)$ separates an isotropic and homogeneous medium from a vacuum, and roughness scatters the incident wave into the vacuum. When the incident polarization is a linear combination of s and p polarizations, depolarization does not occur from 1-D surfaces and the polarization state is retained upon reflection. Consequently, the reflected field components for each polarization ($E_{r,p}$ and $E_{r,s}$) are related to the incident field components ($E_{i,p}$ and $E_{i,s}$) via the following matrix formula.

$$\begin{bmatrix} E_{r,p} \\ E_{r,s} \end{bmatrix} = \begin{bmatrix} c_{pp} & 0 \\ 0 & c_{ss} \end{bmatrix} \begin{bmatrix} E_{i,p} \\ E_{i,s} \end{bmatrix} \tag{1}$$

The matrix elements c_{pp} and c_{ss} (field scattering coefficients) represent the far-field scattered amplitude for incident p and s states of unit amplitude, respectively, for a particular realization of random surfaces. Because cross-polarization terms c_{ps} and c_{sp} are absent, field scattering coefficients c_{pp} and c_{ss} can be independently calculated for pure p or s polarization [14]. The complex modulus of field scattering coefficients $|c_{pp}|^2$ and $|c_{ss}|^2$ is the scattering cross section for corresponding polarization. All the quantities in Eq. (1) are complex numbers and functions of incidence and reflection angles.

The Stokes vector fully describes the polarization state of a monochromatic plane wave by its four elements or parameters, as follows [1,2]:

$$\boldsymbol{S} = \begin{bmatrix} I \\ Q \\ U \\ V \end{bmatrix} = \begin{bmatrix} I_p + I_s \\ I_p - I_s \\ I_{+45} - I_{-45} \\ I_{\mathrm{rhc}} - I_{\mathrm{lhc}} \end{bmatrix} = \begin{bmatrix} \langle E_p E_p^* + E_s E_s^* \rangle \\ \langle E_p E_p^* - E_s E_s^* \rangle \\ \langle E_p E_s^* + E_s E_p^* \rangle \\ i\langle E_p E_s^* - E_s E_p^* \rangle \end{bmatrix} \tag{2}$$

All the preceding properties are obtained from an ensemble average over many surface realizations, denoted by $\langle\,\rangle$. I is the complex modulus of a field $|E|^2$. Subscripts in intensities stand for the linear polarization states of p, s, $+45$ deg, and -45 deg, as well as the circular polarizations of right hand (rhc) and left hand (lhc). Scattering causes the incident Stokes vector to become the scattered Stokes vector, and the Mueller matrix $\mathbf{M}$ links the two Stokes vectors.

$$\begin{bmatrix} I_r \\ Q_r \\ U_r \\ V_r \end{bmatrix} = \begin{bmatrix} m_{11} & m_{12} & 0 & 0 \\ m_{12} & m_{11} & 0 & 0 \\ 0 & 0 & m_{33} & m_{34} \\ 0 & 0 & -m_{34} & m_{33} \end{bmatrix} \begin{bmatrix} I_i \\ Q_i \\ U_i \\ V_i \end{bmatrix} \quad \text{or} \quad \boldsymbol{S}_r = \mathbf{M}\boldsymbol{S}_i \tag{3}$$

The Mueller matrix is generally a 4×4 matrix with 16 elements, but only four independent elements remain for scattering from 1-D rough surfaces [16–18]. Because reflected field components $E_{r,p}$ and $E_{r,s}$ are, respectively, proportional to incident field components $E_{i,p}$ and $E_{i,s}$ by field scattering coefficients c_{pp} and c_{ss}, as shown in Eq. (1), Mueller matrix elements in Eq. (3) can be expressed in terms of field scattering coefficients.

$$\begin{bmatrix} m_{11} \\ m_{12} \\ m_{33} \\ m_{34} \end{bmatrix} = \begin{bmatrix} \frac{1}{2}\langle |c_{pp}|^2 + |c_{ss}|^2 \rangle \\ \frac{1}{2}\langle |c_{pp}|^2 - |c_{ss}|^2 \rangle \\ \frac{1}{2}\langle c_{pp}c_{ss}^* + c_{pp}^* c_{ss} \rangle \\ \frac{i}{2}\langle c_{pp}^* c_{ss} - c_{pp} c_{ss}^* \rangle \end{bmatrix} \tag{4}$$

When incident light is linearly polarized at $+45$ deg, the incident Stokes vector is given by $\boldsymbol{S} = [1, 0, 1, 0]$ and the reflected Stokes vector becomes $\boldsymbol{S}_r = [m_{11}, m_{12}, m_{33}, -m_{34}]$ from Eq. (3). Therefore, the four Mueller matrix elements are, respectively, associated with the reflected Stokes vector elements when incident light with $+45$ deg linear polarization is scattered. Note that $+45$ deg linear polarization is the same as random polarization for scattering from a 1-D rough surface if the plane of incidence is perpendicular to roughness grooves. Meanwhile, the bidirectional reflectance distribution function (BRDF) is often used to describe incident energy distribution after scattering from rough surfaces [2–4]. The element m_{11} also describes energy distribution. Because all the Mueller matrix elements are divided by incident energy $|E_i|^2 L \cos\theta_i$, where L is surface length, the element m_{11} is equal to $f_r \cos\theta_r$.

Often, coherent and incoherent components need to be distinguished for further understanding of radiative properties related to scattering. Phase terms in the field are associated with wave features; for instance, in-phase of two waves leads to constructive interference, whereas out-of-phase of them leads to destructive interference. The coherent components of the Stokes vector elements are expressed by

$$\boldsymbol{S}_{\mathrm{coh}} = \begin{bmatrix} I_{\mathrm{coh}} \\ Q_{\mathrm{coh}} \\ U_{\mathrm{coh}} \\ V_{\mathrm{coh}} \end{bmatrix} = \begin{bmatrix} \langle E_p \rangle\langle E_p^* \rangle + \langle E_s \rangle\langle E_s^* \rangle \\ \langle E_p \rangle\langle E_p^* \rangle - \langle E_s \rangle\langle E_s^* \rangle \\ \langle E_p \rangle\langle E_s^* \rangle + \langle E_s \rangle\langle E_p^* \rangle \\ i\langle E_p \rangle\langle E_s^* \rangle - i\langle E_s \rangle\langle E_p^* \rangle \end{bmatrix} \tag{5}$$

Then, their incoherent components become

$$\boldsymbol{S}_{\mathrm{inc}} = \boldsymbol{S} - \boldsymbol{S}_{\mathrm{coh}} \tag{6}$$

Coherent components include phase terms, because the fields are first averaged $\langle E \rangle$ and then the complex modulus is calculated, as shown in Eq. (5). On the other hand, incoherent components represent an algebraic intensity sum without information about phase. Therefore, only the coherent components account for wave effects on radiative properties.

Surface currents induced by an incident wave generate fields at the surface, and the reflected or scattered field E_r is obtained from the fields at the surface based on Huygens's principle. Huygens's principle states that each element of a wave front may be regarded as the center of a secondary disturbance that gives rise to spherical wavelets, and the position of the wave front at any later time is the envelope of all such wavelets [1,4]. Huygens's principle can be formulated into a general equation, which is derived from Maxwell's equations using Green's function [1,19]. The field at a point $\boldsymbol{r}$ in vacuum is

$$E(\boldsymbol{r}) = E_i(\boldsymbol{r}) + \frac{1}{4\pi}\int_{-\infty}^{\infty} \mathrm{d}S' \left[E_t(\boldsymbol{r}') \frac{\partial G(\boldsymbol{r}, \boldsymbol{r}')}{\partial n'} - G(\boldsymbol{r}, \boldsymbol{r}') \frac{\partial E_t(\boldsymbol{r}')}{\partial n'} \right] \tag{7}$$

In the preceding equation, $\boldsymbol{r}' = [x', \xi(x')]$ indicates a point at the surface. When the unit surface normal is given by

$$\boldsymbol{n}' = [-\xi'(x'), 1]/\sqrt{1 + [\xi'(x')]^2}$$

$$\mathrm{d}S' = -\mathrm{d}x\sqrt{1 + [\xi'(x')]^2}$$

and $\partial/\partial n' = \boldsymbol{n}' \cdot \nabla$. Green's function for a vacuum is given by the zeroth-order Hankel function of the first kind: $G(\boldsymbol{r}, \boldsymbol{r}') = \pi i H_0^{(1)}(k|\boldsymbol{r} - \boldsymbol{r}'|)$. Huygens's principle in Eq. (7) does not alone provide the surface field $E_t(\boldsymbol{r}')$. By virtue of the extinction theorem, the surface fields can be obtained by numerically solving the two coupled integral equations [19,20].

In the Kirchhoff approximation, the surface field $E_t(\boldsymbol{r}')$ is approximated as the field existing on the tangent plane at a considered point, rather than calculated from Huygens's principle and the extinction theorem. Therefore, KA is also known as the tangent plane approximation, and KA is valid for surface roughness with large radii of roughness curvature [21,22]. Many researchers have studied the validity domain of KA, in which KA can replace rigorous solutions of Maxwell's equations [23–25]. The surface field at each point is equal to the incident field multiplied by Fresnel's reflection coefficient calculated at a locally tangent plane.

$$E_t(x) = (1 + R)E_i(x) \tag{8a}$$

$$\frac{\partial E_t(x)}{\partial n} = i(\boldsymbol{k}_i \cdot \boldsymbol{n})(1 - R)E_i(x) \tag{8b}$$

Here, Fresnel's reflection coefficient is denoted by R and depends on the incident polarization state and material properties. The reflected field component for p or s polarization, $E_{r,p}$ or $E_{r,s}$, is determined by Fresnel's reflection coefficient R_p or R_s. With far-field expressions of Green's function and the surface field in Eq. (8), the field $E(\boldsymbol{r})$ in Eq. (7) becomes

$$E(\boldsymbol{r}) = \frac{e^{i(kr-\pi/4)}}{2\sqrt{2\pi kr}} \int_{-\infty}^{\infty} \mathrm{d}S'[(1 + R)(\boldsymbol{n}' \cdot \boldsymbol{k}_r) + (1 - R)(\boldsymbol{n}' \cdot \boldsymbol{k}_i)]e^{i(\boldsymbol{k}_i - \boldsymbol{k}_r)\cdot \boldsymbol{r}'} \tag{9}$$

For rough surfaces following Gaussian statistics, the preceding equation can be further developed with additional assumptions to derive an analytical formula. In the present study, however, the integral in Eq. (9) is numerically evaluated with surface realization, and radiative properties are obtained from the ensemble average in the same fashion as the Monte Carlo method. KA expressed in Eq. (9) is responsible for first-order scattering only. Multiple scattering in KA is usually determined from a geometric-optics viewpoint; that is, by means of a geometric shadowing function or surface realization [21,22]. The characteristic lengths of roughness are the root-mean-square (rms) roughness σ and the autocorrelation length τ. When rms roughness and autocorrelation lengths are sufficiently larger than the wavelength of interest, KA reduces to the geometric-optics approximation. The validity domain of KA has been the subject of a number of studies, involving comparison with rigorous solutions of Maxwell's equations [23–25]. Comparison with the boundary integral method [11] suggests that KA gives satisfactory results for most studied cases, except for element m_{12} when it becomes very small. Although KA is an approximate method, PRTM is compared with KA in the present study because of the relation between KA and geometric-optics approximation. If PRTM could model wave features related to scattering from rough surfaces, it would be consistent with KA rather than any other rigorous method.

Geometric-Optics and Ray-Tracing Methods

In the short wavelength limit $\lambda \to 0$, Maxwell's equations are reduced to an equation that defines a constant optical path, and surfaces of a constant optical path form geometrical wave fronts [1]. Wave propagation direction is normal to wave fronts, and the light ray concept geometrically describes physical laws without dealing with wave features. Therefore, geometric optics is valid when a characteristic length is much larger than the wavelength of incident light. When geometric optics is applied for light scattering from a rough surface, a large number of rays are traced between microfacets

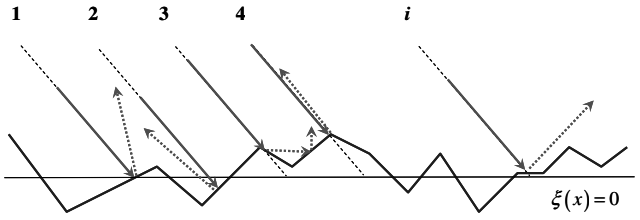

a) Numerical ray tracing with a surface realization

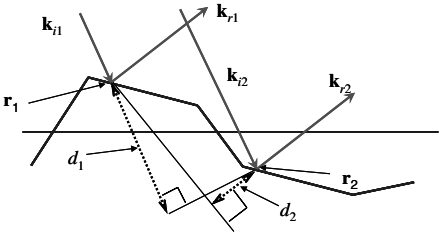

b) Optical path difference between two rays leaving the surface in the same direction

Fig. 2 Ray tracing on a rough surface composed of microfacets.

that compose a rough surface, as shown in Fig. 2a. Ray tracing can be conducted theoretically or numerically. Theoretical ray tracing results in the same analytical formula as that reduced from KA in the short wavelength limit. Numerical ray tracing usually takes advantage of the Monte Carlo method. Because any analytical formula for PRTM by theoretical ray tracing is not available, the present study only uses numerical ray tracing.

In RTM, a rough surface is numerically generated before ray tracing. Then, incident rays are directed toward evenly spaced nodes $(x_i, 0)$ at a mean plane $\xi(x) = 0$, but they intersect with the rough interface at a point different from the target point. The intersection point is numerically determined with a rough surface profile $z = \xi(x)$ and an incident wave vector. At the intersected microfacet, the incident ray is specularly reflected. Each ray is continuously traced for multiple reflections until it leaves the surface without restriking. RTM deals with the intensity and, whenever a ray undergoes reflection, its intensity is reduced by the reflectivity at the intersected microfacet. Rays leaving the surface are collected at discrete angular bins, and the algebraic sum of their final intensities at each bin represents the distribution of scattered energy (i.e., the BRDF). The change of polarization states due to scattering can be considered in RTM [26]. If the reflectivity at a microfacet is calculated based on either p or s polarization, the intensity for the two polarizations I_p or I_s can be separated. As a result, RTM provides only the two Mueller matrix elements m_{11} and m_{12}, and it cannot model coherent components.

Most published works have regarded geometric optics and RTM as identical. However, as discussed with the reflectivity calculation for a smooth surface with thin-film coating, PRTM is applicable when a characteristic length is smaller than the wavelength, unlike RTM. When PRTM is extended to scattering from rough surfaces, the reflected ray direction is determined in the same fashion as in RTM, that is, specular reflection. However, the amplitude and phase of incident rays are traced in PRTM. The amplitude is multiplied by complex Fresnel's reflection coefficient for every reflection, depending on the incident polarization. The phase is considered based on the relative difference of the optical paths. Figure 2b shows the path difference of two rays leaving the surface in the same direction, d_1 and d_2. The phase difference between them becomes $\delta = \delta_1 - \delta_2 = (\boldsymbol{k}_i - \boldsymbol{k}_r) \cdot (\boldsymbol{r}_1 - \boldsymbol{r}_2)$, and any increase in traveling distances due to multiple scattering can be included in the phase difference. Because only the relative path difference is important, path differences are calculated using a reference point 0, 0. The amplitude multiplied by $\exp(i\delta)$ results in a complex number, which can be interpreted as the reflected field of an incident ray. Because the reflected electric field can be modeled from the sum of complex numbers after many rays are traced and polarization is considered,

PRTM allows the study of all four Mueller matrix elements, including the coherent components.

PRTM does not observe energy conservation when applied for rough surfaces, whereas RTM always does. Even for perfectly conducting surfaces, the directional hemispherical reflectance obtained from PRTM is not unity. Radiative properties calculated with PRTM depend on surface length or node numbers. PRTM cannot be used to calculate any absolute values of radiative properties, only their relative values. From a KA viewpoint, an incident wave generates current sources for spherical wavelets at an intersected microfacet, and both the incident field amplitude and Fresnel's reflection coefficient determine current source strength. The spherical wavelets affect all points in a vacuum. KA considers all the spherical wavelets generated at the rough surface according to Huygens's principle when the reflected field is calculated; refer to the integration in Eq. (9). In PRTM, on the other hand, an incident wave generates sources with the same strength as KA. However, the sources give rise to rays instead of spherical wavelets, and the light ray concept is constantly maintained after reflection. As a result, PRTM does not obey Huygens's principle and thus energy conservation. Meanwhile, when PRTM is applied for a smooth surface, the wave vector difference $\boldsymbol{k}_i - \boldsymbol{k}_r$ is parallel to the z axis because of specular reflection. The position vector difference $\boldsymbol{r}_1 - \boldsymbol{r}_2$ is parallel to the x axis, because $\xi(x) = 0$. Therefore, the phase difference $\delta = (\boldsymbol{k}_i - \boldsymbol{k}_r) \cdot (\boldsymbol{r}_1 - \boldsymbol{r}_2)$ vanishes. For smooth surfaces, PRTM inherently obeys Huygens's principle, and energy is conserved.

Results and Discussion

For the evaluation of PRTM, the four Mueller matrix elements are compared with 1-D silicon and gold surfaces for which roughness follows Gaussian statistics. The incidence wavelength of 2 μm is used, and the complex refractive indices of silicon and gold are $\tilde{n} = 3.449$ and $\tilde{n} = 0.850 + 12.6i$, respectively [27]. Silicon and gold surfaces, respectively, represent dielectric and highly conducting surfaces. Because the KA expression in Eq. (9) does not account for multiple scattering, the roughness parameters are selected so that multiple scattering becomes negligible. Surface lengths range from 60λ to 180λ, and each surface is divided into 512 nodes. A set of the four matrix elements is calculated with a numerically generated surface, and all presented results are averaged over calculations obtained with 2000 surfaces. As a result, relative standard deviations of the three methods are less than 15% when the calculated values are greater than 10^{-5}. For comparison with KA and RTM, PRTM calculations must be normalized. Bruce [14] normalized the matrix element m_{11} by fitting with measurements at an arbitrary reflection angle and the other elements by dividing with m_{11}. In the present study, however, all the elements are normalized with the directional hemispherical reflectance obtained from KA. Note that KA and RTM yield the same directional hemispherical reflectance as long as only first-order scattering is involved, even if they predict different BRDFs [12].

Figure 3 shows Mueller matrix elements for a rough silicon surface with $\sigma/\lambda = 0.3$ and $\tau/\lambda = 6$ when $\theta_i = 30$ deg. The element m_{11} is the reflected intensity sum over p and s polarizations and contains the same information as the BRDF at randomly polarized incidence. On the other hand, the element m_{12} represents the reflected intensity difference between p and s polarizations. The intensity for s polarization is larger than that for p polarization, and thus the element m_{12} is negative in Fig. 3. Because a small σ/τ ratio indicates small roughness slopes, the difference between R_p and $-R_s$ is insignificant and c_{pp} is nearly equal to $-c_{ss}$, as well. As a result, no appreciable difference between m_{11} and $-m_{33}$ is observed. The element m_{34} is related to the reflected intensity difference between right-handed and left-handed circular polarizations, as shown in Eq. (2). Circular polarizations occur when a linearly polarized light is reflected from an absorbing material for which the refractive index has a nonzero imaginary part. Therefore, m_{34} calculation with a dielectric silicon surface results in only numerical fluctuations, so they are not presented in Fig. 3.

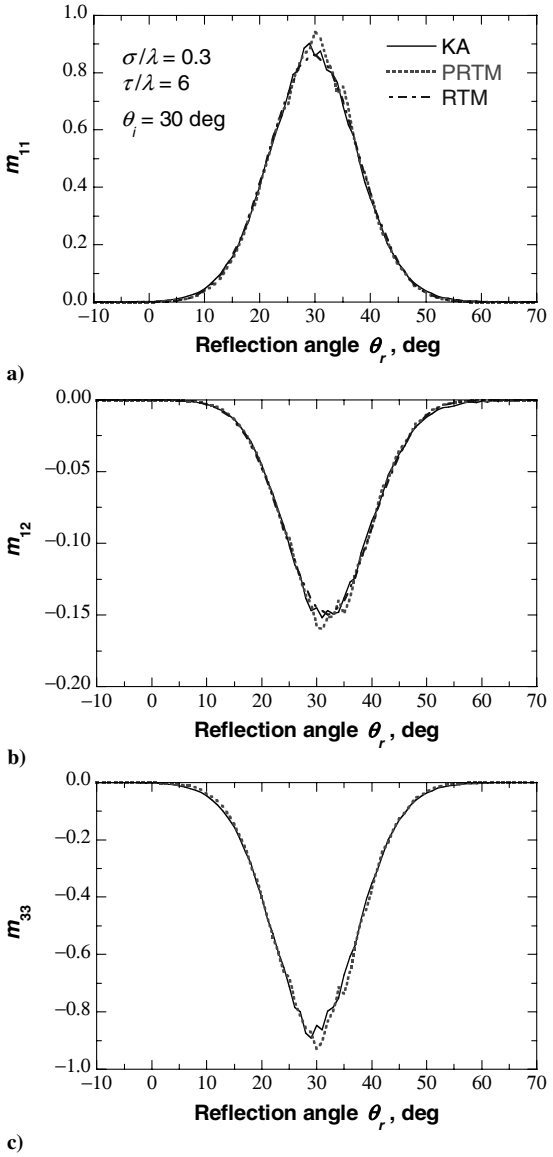

Fig. 3 Mueller matrix elements for a silicon surface with $\sigma/\lambda = 0.3$ and $\tau/\lambda = 6$ when $\theta_i = 30$ deg: a) m_{11}, b) m_{12}, and c) m_{33}. The elements are calculated with KA, PRTM, and RTM.

Because the roughness parameters in Fig. 3 indicate a large rms radius of roughness curvature $\tau^2/\sqrt{12}\sigma$, KA is valid for the studied surface [23–25]. The two elements m_{11} and m_{12} from RTM are compared in Figs. 3a and 3b. For all compared elements, PRTM agrees with KA and RTM within the numerical uncertainties. Comparisons also demonstrate that RTM is valid for the given surface. Even though the rms roughness is smaller than the wavelength ($\sigma/\lambda = 0.3$), the autocorrelation length is large enough to validate RTM. Good agreement between RTM and KA suggest that, at the given rms roughness, rays reflected in the same direction possess considerable variation in their phase differences. If an rms value of phase difference is much larger than π, the distribution of phase difference, whatever it is, is equivalent to a uniform distribution from $-\pi$ to π [21]. The uniform distribution of phase difference means that wave effects are cancelled out. When coherent and incoherent components shown in Fig. 3 are divided according to Eqs. (5) and (6), it is confirmed that coherent components are negligibly small, whereas incoherent components are dominant.

After the incidence angle is changed from $\theta_i = 30$ deg to $\theta_i = 0$ deg, a similar comparison with the same silicon surface as in Fig. 3 is presented in Fig. 4. Again, the difference between m_{11} and $-m_{33}$ is not distinguishable, and the element m_{33} is not presented. Figure 4a shows that agreement between KA and PRTM in the

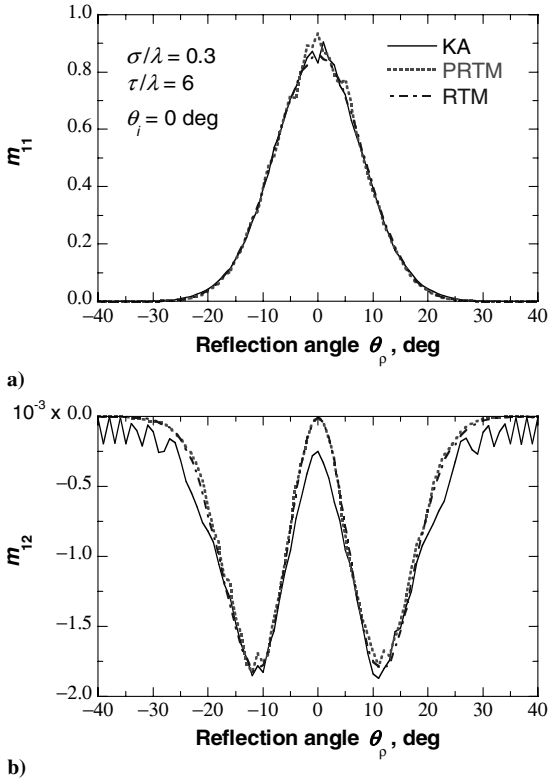

Fig. 4 Mueller matrix elements for a silicon surface with $\sigma/\lambda = 0.3$ and $\tau/\lambda = 6$ when $\theta_i = 0$ deg: a) m_{11} and b) m_{12}.

element m_{11} is still good, although a bell-shaped distribution remains, as in Fig. 3a. However, PRTM slightly deviates from KA around $\theta_r = 0$ deg and $|\theta_r| > 20$ deg in Fig. 4b, although the fixed roughness parameters indicate negligible wave features. KA oscillates at large reflection angles, but PRTM tends to match with RTM without any oscillation. Despite the small deviations in Fig. 4b, the element m_{12} is small, due to the small intensity difference of reflected rays between p and s polarizations at $\theta_i = 0$ deg, and PRTM generally follows the trend of KA. Therefore, Figs. 3 and 4 suggest that PRTM is essentially the same as KA and identical to RTM for the surfaces with large characteristic lengths.

Figure 5 shows Mueller matrix elements for a silicon surface with $\sigma/\lambda = 0.1$ and $\tau/\lambda = 2$ when $\theta_i = 0$ deg. Both roughness parameters are scaled down by a factor of three, compared with those in Figs. 3 and 4. KA reveals narrow peaks for all the elements in Fig. 5, unlike the results in Figs. 3 and 4. PRTM also predicts narrow peaks in the elements m_{11} and m_{33}, but not in the element m_{12}. However, the peaks predicted by PRTM are smaller than those predicted by KA, approximately by 46% in Figs. 5a and 5c. Furthermore, PRTM deviates from KA in angular regions other than the narrow peaks, whereas it follows the distribution of RTM for the element m_{11}. Figure 5b indicates that PRTM completely differs from KA and better agrees with RTM, although m_{12} values are relatively small. Despite the reduction of roughness parameters from Fig. 4 and 5, the elements m_{11} and m_{12} calculated by RTM do not change except due to numerical fluctuations. The invariance of radiative properties at a constant σ/τ ratio is a feature of RTM. However, the appearance of the narrow peaks in some elements demonstrates that PRTM is not identical to RTM at small roughness parameters.

For the results in Fig. 5, coherent and incoherent components are divided and presented in Fig. 6. Note that RTM does not allow the division into coherent and incoherent components. Both KA and PRTM indicate that the narrow peaks in all the elements originate from coherent components, as a result of wave effects. However, PRTM does not predict accurately incoherent components as well as coherent components in Figs. 6a and 6c. For the element m_{12}, moreover, PRTM does not show any noticeable contribution of coherent components. With the same surface, coherent and

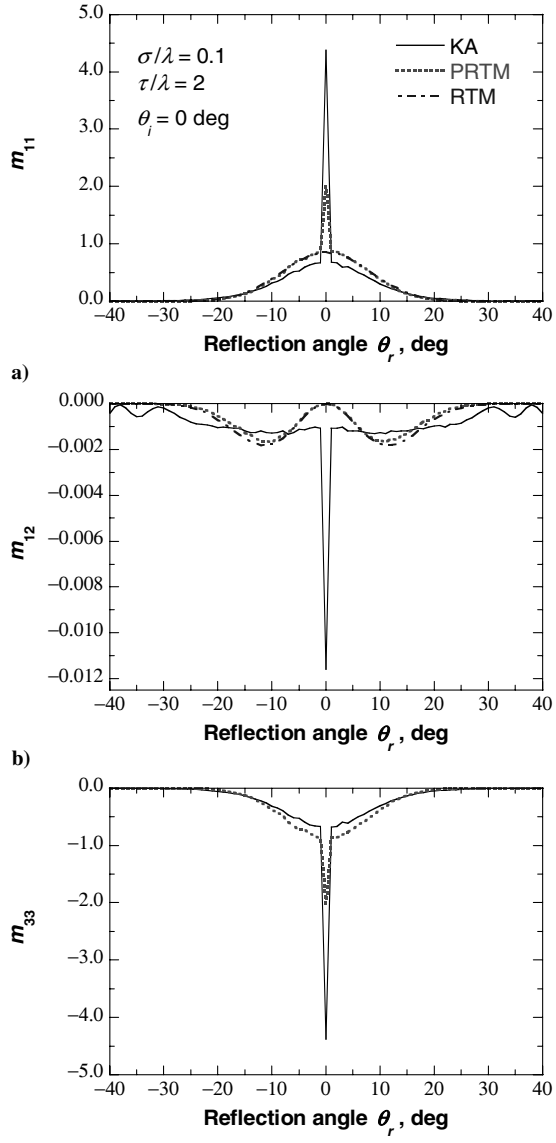

Fig. 5 Mueller matrix elements for a silicon surface with $\sigma/\lambda = 0.1$ and $\tau/\lambda = 2$ when $\theta_i = 0$ deg: a) m_{11}, b) m_{12}, and c) m_{33}.

incoherent components are additionally calculated at oblique incidence angles (not presented). In those cases, PRTM predicts coherent peaks for the element m_{12}, which are smaller than those of KA, similar to the comparisons in Figs. 6a and 6c. Consequently, PRTM does not account for wave features accurately for rough surfaces, although it predicts partially coherent components. PRTM may fail to predict coherent components for some elements. In fact, the distinction of coherent components has led to various applications. For instance, coherent and incoherent components are, respectively, approximated as specular and diffuse components of the reflectivity in many radiative heat transfer problems [3,4]. Only coherent components in the specular direction can be used to characterize roughness parameters, optical constants, or thickness of a material [21,28,29]. PRTM may not be applied for such applications because of its inaccurate prediction for coherent components.

Up to now, the Mueller matrix was compared for silicon, which is a dielectric material at $\lambda = 2$ μm. Comparisons made with a gold surface are shown in Figs. 7 and 8. The reflectivity of a smooth gold surface is 0.98 at $\lambda = 2$ μm for $\theta_i < 30$ deg, and the gold surface may be regarded as a perfectly conducting surface. The elements m_{11} and m_{34} for normal incidence are compared in Fig. 7 with the same roughness parameters as in Fig. 4. The element m_{33} is not presented because of negligible difference between m_{11} and $-m_{33}$.

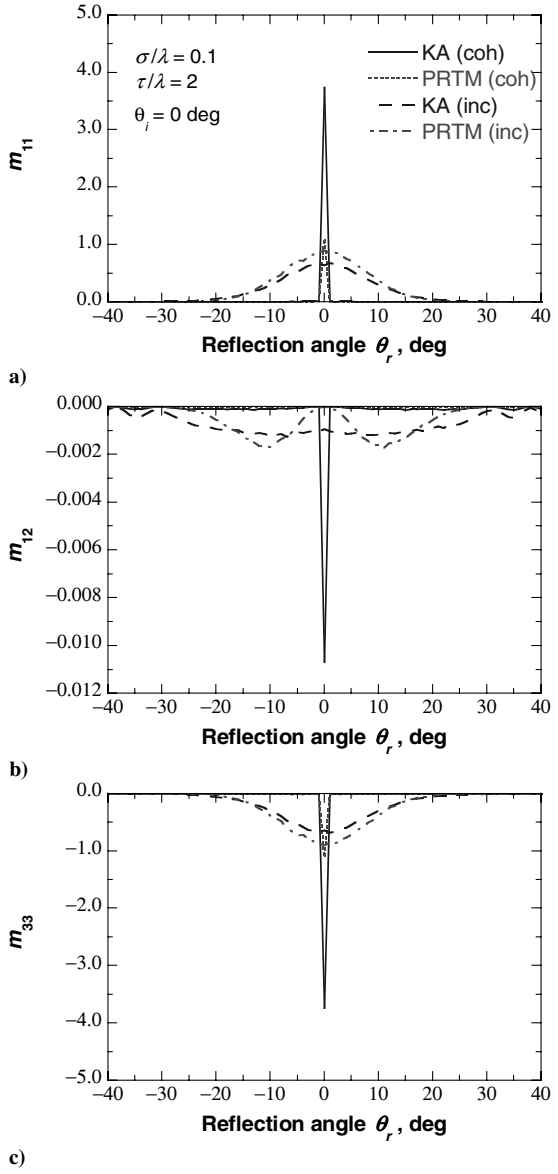

Fig. 6 Coherent and incoherent components of the results in Fig. 5: a) m_{11}, b) m_{12}, and c) m_{33}.

Furthermore, the small intensity difference between p and s polarizations at $\theta_i = 0$ deg results in very small m_{12} that is not accurate enough to be presented. The results in Fig. 7 have negligible coherent components, due to the large rms roughness. Figure 7a shows that the three methods agree well for m_{11}. Compared with Fig. 4a, the angular dependence of element m_{11} is very similar for gold and silicon surfaces. The only difference is the large values in Fig. 7a that are due to the large reflectivity of gold. Interestingly, the element m_{34} for the gold surface in Fig. 7b exhibits similar variations and magnitude as the element m_{12} for the silicon surface in Fig. 4b. In both cases, only KA results oscillate at large incidence angles and there exists some difference between KA and PRTM around $\theta_r = 0$ deg. It can be concluded from Figs. 4 and 7 that PRTM is essentially the same as KA for all the four elements in the incoherent limit.

Figure 8 shows coherent and incoherent components of the elements m_{11} and m_{34} for a gold surface with $\sigma/\lambda = 0.1$ and $\tau/\lambda = 2$ when $\theta_i = 0$ deg. Because of the small rms roughness, coherent peaks appear for both elements in the KA calculation, this is also true for the element m_{33}. Similarly to the comparisons in Fig. 6, a narrow peak in the element m_{11} calculated with PRTM is smaller than that calculated with KA. For the element m_{34}, PRTM disagrees with KA when predicting negligibly small coherent components. If the incidence angle is oblique (not presented), PRTM shows a coherent

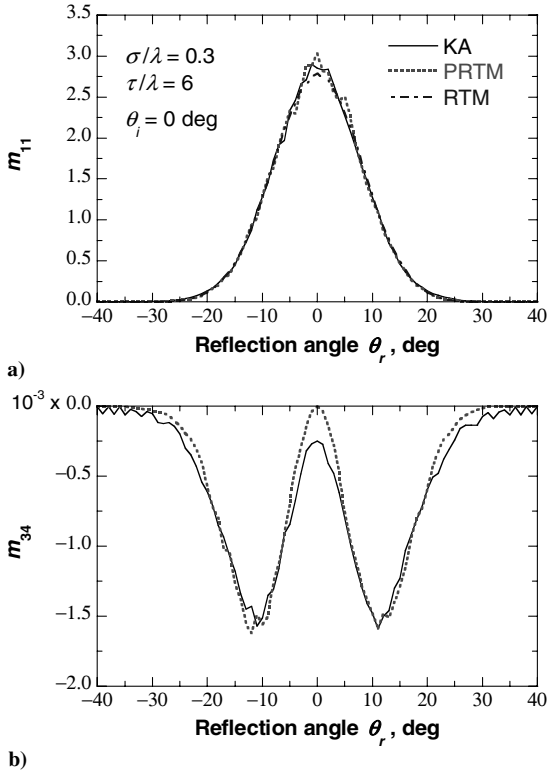

Fig. 7 Mueller matrix elements for a gold surface with $\sigma/\lambda = 0.3$ and $\tau/\lambda = 6$ when $\theta_i = 0$ deg: a) m_{11} and b) m_{34}.

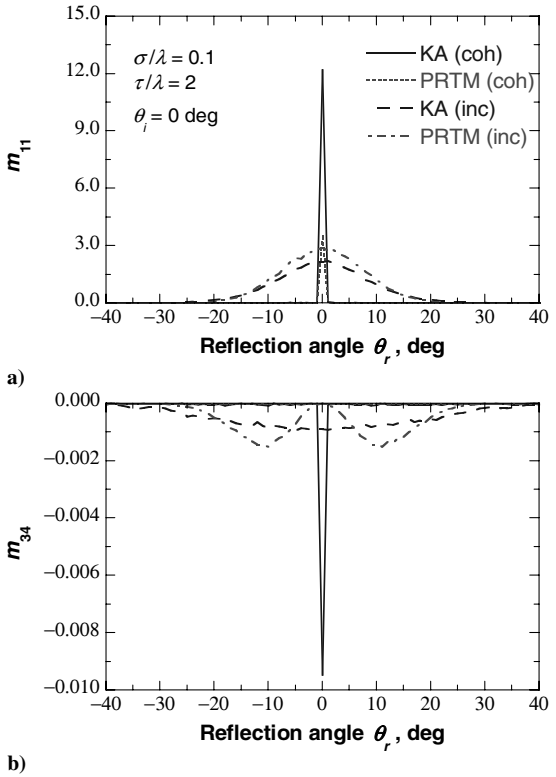

Fig. 8 Coherent and incoherent components of Mueller matrix elements for a gold surface with $\sigma/\lambda = 0.1$ and $\tau/\lambda = 2$ when $\theta_i = 0$ deg: a) m_{11} and b) m_{34}.

peak in the element m_{34}, which is still underpredicted. Regardless of surface materials, PRTM does not predict the Mueller matrix elements accurately when wave features are involved. Furthermore, PRTM may completely fail to predict the elements m_{12} and m_{34}, depending on materials and incidence angles.

Conclusions

This work assesses the applicability of PRTM for scattering from rough surfaces by comparing the four Mueller matrix elements of 1-D dielectric and highly reflecting surfaces calculated with PRTM, KA, and RTM. When the rms roughness is large and thus wave features are negligible, PRTM is essentially the same as KA for all the elements and also the same as RTM for elements m_{11} and m_{12}. When the rms roughness is small, KA shows that wave effects result in narrow specular peaks for all the elements. However, PRTM always underpredicts the specular peaks and deviates from KA in other angular regions. Furthermore, PRTM does not show any coherent components in m_{12} for dielectric or in m_{34} for metallic surfaces. Therefore, PRTM is not applicable for light scattering from rough surfaces to fully account for wave features at small characteristic lengths, although it predicts partial coherent components. PRTM is just a useful method to model the reflected fields within the geometric-optics domain. However, due to the violation of energy conservation, PRTM does not yield absolute radiative properties and its calculation must be normalized properly. This research facilitates a fundamental understanding of radiative interactions with a rough surface with small length scales and helps in the selection of a suitable tool to tackle light scattering from rough surfaces.

Acknowledgments

This work was supported by the National Science Foundation, under CTS-0500113. The authors thank Pei-feng Hsu of the Florida Institute of Technology and Keunhan Park and Bong Jae Lee of the Georgia Institute of Technology for valuable discussions.

References

[1] Born, M., and Wolf, E., *Principles of Optics*, 7th (expanded) ed., Cambridge Univ. Press, Cambridge, England, U.K., 1999, Chap. 3.

[2] Modest, M. F., *Radiative Heat Transfer*, McGraw–Hill, New York, 1993.

[3] Siegel, R., and Howell, J. R., *Thermal Radiation Heat Transfer*, 4th ed., Taylor and Francis, New York, 2002, Chaps. 3, 5, 9.

[4] Mahan, J. R., *Radiation Heat Transfer: A Statistical Approach*, Wiley, New York, 2002, Chaps. 3, 4.

[5] Howell, J. R., and Perlmutter, M., "Monte Carlo Simulation of Thermal Transfer Through Radiant Media Between Gray Walls," *Journal of Heat Transfer*, Vol. 86, No. 1, 1964, pp. 116–122.

[6] Torrance, K. E., and Sparrow, E. M., "Theory for Off-Specular Reflection from Roughened Surfaces," *Journal of the Optical Society of America*, Vol. 57, No. 9, 1967, pp. 1105–1114.

[7] Toor, J. S., and Viskanta, R., "A Numerical Experiment of Radiant Heat Interchange by Monte Carlo Method," *International Journal of Heat and Mass Transfer*, Vol. 11, No. 5, 1968, pp. 883–897.

[8] Tang, K., and Buckius, R. O., "A Statistical Model of Wave Scattering from Random Rough Surfaces," *International Journal of Heat and Mass Transfer*, Vol. 44, No. 21, 2001, pp. 4059–4073.

[9] Lee, H. J., Lee, B. J., and Zhang, Z. M., "Modeling the Radiative Properties of Semitransparent Wafers with Rough Surfaces and Thin-Film Coatings," *Journal of Quantitative Spectroscopy and Radiative Transfer*, Vol. 93, Nos. 1–3, 2005, pp. 185–194.

[10] Tang, K., Dimenna, R. A., and Buckius, R. O., "Regions of Validity of the Geometric Optics Approximation for Angular Scattering from Very Rough Surfaces," *International Journal of Heat and Mass Transfer*, Vol. 40, No. 1, 1997, pp. 49–59.

[11] Zhu, Q. Z., Lee, H. J., and Zhang, Z. M., "The Validity of Using Thin-Film Optics in Modeling the Bidirectional Reflectance of Coated Rough Surfaces," *Journal of Thermophysics and Heat Transfer*, Vol. 19, No. 4, 2005, pp. 548–557.

[12] Ghmari, F., Ghbara, T., Laroche, M., Carminati, R., and Greffet, J. J., "Influence of Microroughness on Emissivity," *Journal of Applied Physics*, Vol. 96, No. 5, 2004, pp. 2656–2664.

[13] Ghmari, F., Sassi, I., and Sifaoui, M. S., "Directional Hemispherical Radiative Properties of Random Dielectric Rough Surfaces," *Waves in Random and Complex Media*, Vol. 15, No. 4, 2005, pp. 469–486.

[14] Bruce, N. C., "Scattering of Light from Surfaces with One-Dimensional Structure Calculated by the Ray-Tracing Method," *Journal of the Optical Society of America, A: Optics, Image Science and Vision*, Vol. 14, No. 8, 1997, pp. 1850–1858.

[15] Bruce, N. C., "Calculations of the Mueller Matrix for Scattering of Light from Two-Dimensional Surfaces," *Waves in Random Media*, Vol. 8, No. 1, 1998, pp. 15–28.

[16] O'Donnell, K. A., and Knotts, M. E., "Polarization Dependence of Scattering from One-Dimensional Rough Surfaces," *Journal of the Optical Society of America, A: Optics, Image Science and Vision*, Vol. 8, No. 7, 1991, pp. 1126–1131.

[17] Videen, G., Aslan, M. M., and Mengüç, M. P., "Characterization of Metallic Nano-Particles via Surface Wave Scattering: A. Theoretical Framework and Formulation," *Journal of Quantitative Spectroscopy and Radiative Transfer*, Vol. 93, Nos. 1–3, 2005, pp. 195–206.

[18] Aslan, M. M., Mengüç, M. P., and Videen, G., "Characterization of Metallic Nano-Particles via Surface Wave Scattering, B: Physical Concept and Numerical Experiments," *Journal of Quantitative Spectroscopy and Radiative Transfer*, Vol. 93, Nos. 1–3, 2005, pp. 207–217.

[19] Tsang, L., Kong, J. A., and Ding, K.-H., *Scattering of Electromagnetic Waves. Theories and Applications*, Wiley, New York, 2000, Chap. 2.

[20] Sanchez-Gil, J. A., and Nieto-Vesperinas, M., "Light Scattering from Random Rough Dielectric Surfaces," *Journal of the Optical Society of America, A: Optics, Image Science and Vision*, Vol. 8, No. 8, 1991, pp. 1270–1286.

[21] Beckmann, P., and Spizzichino, A., *The Scattering of Electromagnetic Waves from Rough Surfaces*, Artechhouse, Norwood, MA, 1987, Chaps. 5, 7.

[22] Ogilvy, J. A., *Theory of Wave Scattering from Random Rough Surfaces*, Adam Hilger, Bristol, England, U.K., 1991, Chap. 4.

[23] Chen, M. F., and Fung, A. K., "A Numerical Study of the Regions of Validity of the Kirchhoff and Small Perturbation Rough Surface Scattering Models," *Radio Science*, Vol. 23, No. 2, 1988, pp. 163–170.

[24] Thorsos, E. I., "The Validity of the Kirchhoff Approximation for Rough Surface Scattering Using a Gaussian Roughness Spectrum," *Journal of the Acoustical Society of America*, Vol. 83, No. 1, 1988, pp. 78–92.

[25] Dimenna, R. A., and Buckius, R. O., "Quantifying Specular Approximations for Angular Scattering from Perfectly Conducting Random Rough Surfaces," *Journal of Thermophysics and Heat Transfer*, Vol. 8, No. 3, 1994, pp. 393–399.

[26] Lee, H. J., Chen, Y.-B., and Zhang, Z. M., "Directional Radiative Properties Anisotropic Rough Silicon and Gold Surfaces," *International Journal of Heat and Mass Transfer*, Vol. 49, Nos. 23–24, 2006, pp. 4482–4495.

[27] Palik, E. D., *Handbook of Optical Constants of Solids*, Academic Press, Orlando, FL, 1985, pp. 286–295, 547–569.

[28] Mitsas, C. L., and Siapkas, D. I., "Generalized Matrix-Method for Analysis of Coherent and Incoherent Reflectance and Transmittance of Multilayer Structures with Rough Surfaces, Interfaces, and Finite Substrates," *Applied Optics*, Vol. 34, No. 10, 1995, pp. 1678–1683.

[29] Lee, B. J., Khuu, V. P., and Zhang, Z. M., "Partially Coherent Spectral Transmittance of Dielectric Thin Films with Rough Surfaces," *Journal of Thermophysics and Heat Transfer*, Vol. 19, No. 3, 2005, pp. 360–366.